THE LANCET
Planetary Health

Supplementary appendix

This appendix formed part of the original submission and has been peer reviewed. We post it as supplied by the authors.

Supplement to: Nice KA, Thompson J, Zhao H, et al. Effects of city design on transport mode choice and exposure to health risks during and after a crisis: a retrospective observational analysis. *Lancet Planet Health* 2025; **9:** e467–79.

City designs affect transport mode choice and exposure to health risks during and after a crisis: a global observational study

Kerry A. Nice[a,∗∗], Jason Thompson[d,c,∗∗], Haifeng Zhao[a], Sachith Seneviratne[a], Belen Zapata-Diomedi[e], Leandro Garcia[f,m], Ruth F. Hunter[f], Rodrigo Siqueira Reis[g], Pedro C. Hallal[h,l], Christopher Millett[i,j,k], Ruoyu Wang[f], Mark Stevenson[a,b]

[a]*Transport, Health, and Urban Systems Research Lab, Faculty of Architecture, Building, and Planning, University of Melbourne, VIC, Australia*

[b]*Faculty of Engineering and Information Technology and the Melbourne School of Population and Global Health, University of Melbourne, VIC, Australia*

[c]*Centre for Human Factors and Sociotechnical Systems University of the Sunshine Coast, Queensland, Australia*

[d]*Department of Psychiatry, Faculty of Medicine, Dentistry and Health Sciences, The University of Melbourne, VIC, Australia*

[e]*Healthy Liveable Cities Lab, Centre for Urban Research, RMIT University, Melbourne, Australia*

[f]*Centre for Public Health, Queen's University Belfast, Institute of Clinical Sciences B, Belfast, Northern Ireland, UK*

[g]*Washington University, St. Louis, Missouri, US*

[h]*Department of Kinesiology and Community Health, University of Illinois Urbana-Champaign*

[i]*Public Health Policy Evaluation Unit, School of Public Health, Imperial College London, London, United Kingdom*

[j]*NOVA National School of Public Health, Public Health Research Centre, Comprehensive Health Research Center (CHRC), NOVA University Lisbon, Lisbon, Portugal*

[k]*Instituto de Estudos para Pol´ıticas de Sau´de (IEPS), Sa˜o Paulo, Brazil*

[l]*Postgraduate Program in Epidemiology, Federal University of Pelotas, Brazil*

[m]*Physical Activity Epidemiology Group, University of Sa˜o Paulo, Sa˜o Paulo, Brazil*

Appendix

Table of Contents

Appendix 1

Figure S1: Overview of the study's methodology, combining mobility and pollution data for 507 global cities during 2020 to demonstrate city design can enable or constrain public health measures leading to either better or worse disease and transportation injury risk. 2

Figure S2: Location of the 507 cities used in this study. 3

Box S3: Graph neural network 3

Box S4: Air pollution and city mobility changes during COVID-19 4

Table S1: Relative health risks (and 95% confidence interval) associated with air pollution reductions across continents and phases. Numbers >1 indicate increased health risks. 5

Figure S5: An overview of observed modal shift from public transit to private motor vehicles observed during 2020 for all analysed cities highlighting an increased reliance on private vehicle use over public transit during the course of the COVID-19 pandemic. Values >0 indicate a proportional replacement of public transit trips to private vehicles for individual cities in comparison to pre-pandemic conditions. 6

Figure S6: Nine global city design types identified in Thompson et al. (2020)[6] for the 507 cities used in this study. City locations and grid references correspond to those in Figure 1........ 7

Figure S7: Mean reported COVID-19 cases per 100,000 population across continents in 2020 for the Early, Mid-Crisis, and Recovery pandemic phases with error bars representing standard deviations across countries within regions. 8

Figure S8: Changes in total road traffic fatalities among the 43 member countries contributing to the International Traffic Safety Data and Analysis Group (IRTAD) showing a post-pandemic (2020-2021) rebound (figure adapted from[24]). 8

Figure S9: Number of the largest 1632 global cities in countries and the number of cities after excluding cities with insufficient data in Africa. Text annotations show proportions of total (in percents) for each country. 9

Figure S10: Number of the largest 1632 global cities in countries and the number of cities after excluding cities with insufficient data in Asia. Text annotations show proportions of total (in percents) for each country. 9

Figure S11: Number of the largest 1632 global cities in countries and the number of cities after excluding cities with insufficient data in Europe. Text annotations show proportions of total (in percents) for each country. 10

Figure S12: Number of the largest 1632 global cities in countries and the number of cities after excluding cities with insufficient data in North America. Text annotations show proportions of total (in percents) for each country. 10

Figure S13: Number of the largest 1632 global cities in countries and the number of cities after excluding cities with insufficient data in Oceania. Text annotations show proportions of total (in percents) for each country........ 11

Figure S14: Number of the largest 1632 global cities in countries and the number of cities after excluding cities with insufficient data in South America. Text annotations show proportions of total (in percents) for each country. 11

References........ 12

∗Principal corresponding author

∗∗Authors contributed equally

Email address: kerry.nice@unimelb.edu.au (Kerry A. Nice)

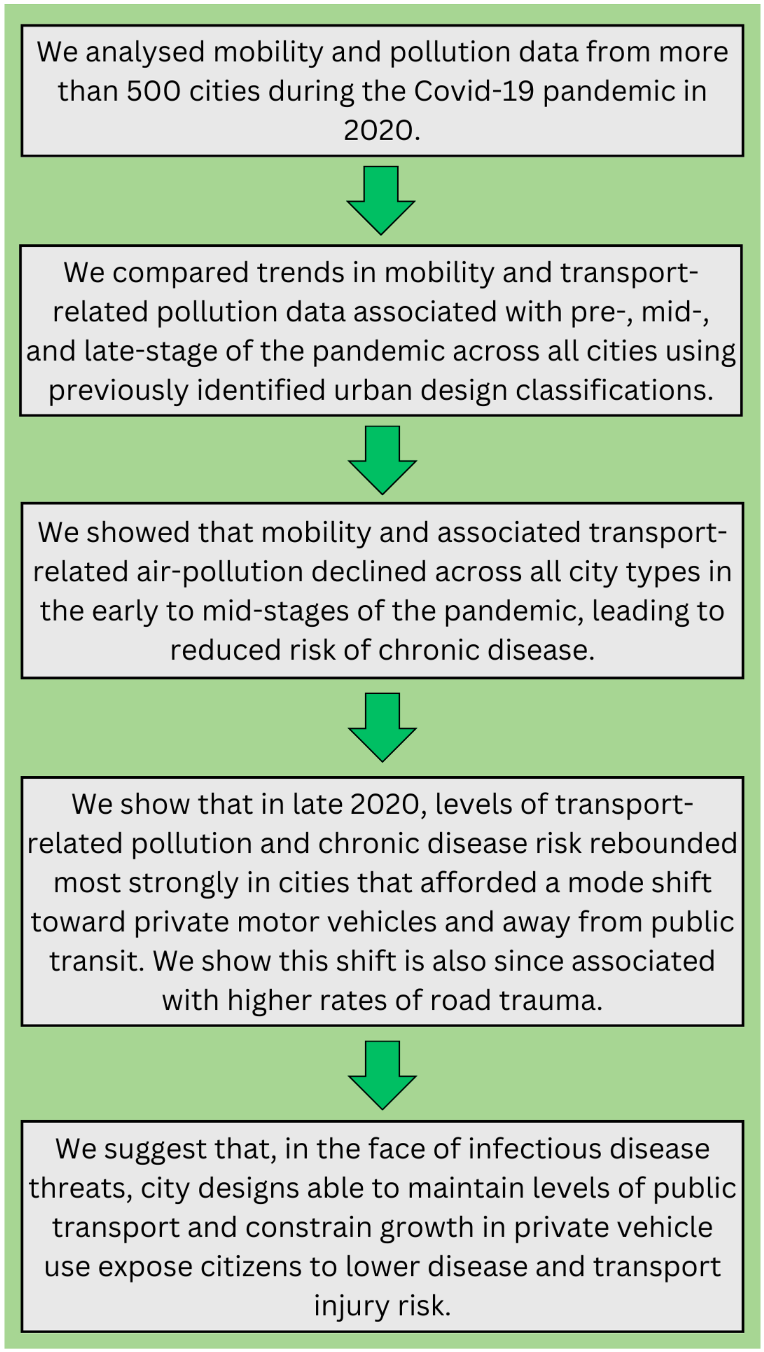

Figure S1: Overview of the study's methodology, combining mobility and pollution data for 507 global cities during 2020 to demonstrate city design can enable or constrain public health measures leading to either better or worse disease and transportation injury risk.

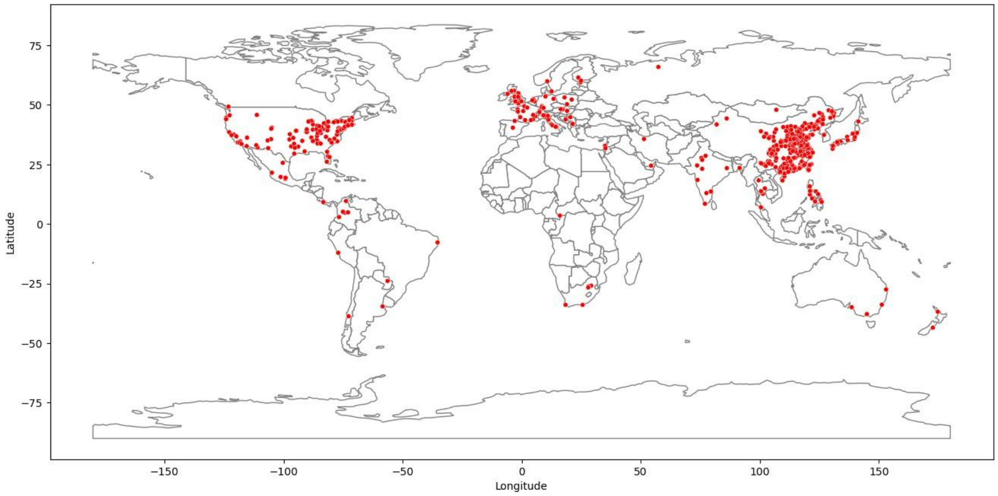

Figure S2: Location of the 507 cities used in this study.

Growing availability of spatial big data have led to increasing usage of graph neural networks (GNN) in urban studies, using urban street networks to explore the urban form, discover urban growth patterns and socioeconomic statuses, derive the functions of urban features in street view imagery, or to enable the fusion of multiple sources of information to uncover the cultural characteristics of neighbourhoods from street view imagery [1–5]. GNNs work by forming high-dimensional hypotheses that can represent input data; in this case, road networks, public transit networks, and active transport networks (e.g., walking and cycling paths) derived from OSM data. In the context of understanding mobility patterns, the utilisation of OSM data offers significant advantages over sampled imagery data used in previous studies (e.g. [6,7]) due to OSM data's high density and its capacity to represent features of an entire city, rather than relying upon sampled data from locations across cities. To conduct global studies, OSM has proven to be an essential source of data, especially in data poor regions of the world where it might be the only source of that information. The coverage of cities analysed are shown in Figure S2 and Figures S9-S14.

We trained a graph neural network using self-supervised learning; a method demonstrated to capture urban form comparably to supervised learning [7]. Importantly, this allows the graph neural network used here to represent the data without requiring a labelled output to the neural network, as used in a recent study [6]. Masked Auto-encoding (MAE) was used as the training objective of the graph neural network. This objective has demonstrated effective performance in neural networks across various data modalities such as graphs [11], images [12], graphs represented as images [13] and text [14]. MAE trains the neural network by 'masking' part of the input data, then tasking the model with predicting the masked (unknown) portion. Here, we masked both road (edge) features–such as length, start and end locations of roads–as well as node features such as latitude and longitude. The model then attempted to predict surrounding OSM sections from the remainder of the available sample.

The results of this analysis were then converted to a t-SNE [15] graph which organised the average value of each city's OSM sample in a 2-dimensional plane where the distance between cities on the graph represented their similarities across urban characteristics (see Figure 1). t-distributed stochastic neighbour embedding (t-SNE) is a method to visualise higher-dimension data by reducing it to two or three dimensions.

Box S3: Graph neural network

Starting with the list of the largest cities in the world, taken from the 2015 United Nations' World Urbanization Prospects report [16], Thompson et al. (2020) [6] classified 1692 cities into types based on urban design characteristics and the associations of these types to road transport injury. This study and Wijnands et al. (2022) [17] also used this list as a starting point and collected data (OSM data (Box S3) and pollution data (below)), to maximise the coverage of as many of these cities as possible.

The pollution data used in this study was derived from data generated by Wijnands et al. (2022) [17]. That study found remote-sensing data to be of insufficient resolution (often 10km) to detect pollution anomalies of NO_2, $PM_{2.5}$, PM_{10}, and O_3 during 2020. Instead, ground-based observations were collected from as many locations across approximately 900 cities, supplied by the environmental protection agencies for 132 countries. Using city-level daily averages of hourly pollution observations from 2015-2019, combined with ERA5[18] weather observations for this same period, individual pollutant and city specific XGBoost models were trained and validated as suitable to predict daily air pollution levels in each city. Cities with less than 365 training samples over 2015-2020 and less than 330 measurements in 2020 were not included in the set of 900 cities. Features selected for the model training include air temperature on day t and days t-3, 2, and 1, net solar radiation on day t and days t-3, 2, and 1, total precipitation on day t and sum of days t-3, 2, and 1, wind speed on day t, wind direction on day t, leaf area index on day t, and year as well as the daily pollutant levels. Excluded features included day of week and day of year, so that those variables could be examined in the later analysis. The resulting models could account for seasonal and long-term trends as well as daily conditions and anomalies can be attributed to mobility restrictions and how they contribute to pollution levels. Using 2020 weather observations, 2020 pollution levels in the absence of a pandemic (counterfactual business as usual) were predicted and anomalies calculated.

Apple [19] and Google [20] provided mobility indexes in 2020. Apple's index calculates differences in map requests for modes of walking, driving, or public transit over a January 2020 baseline provided as a ratio. Google generated an index using phone-tracking-based changes in mobility across several types of locations, including retail and recreation, grocery stores and pharmacies, parks, public transit stations, workplaces, and private residences. These daily indexes were linked to the 507 cities with available air pollution data with changes representing percentage differences in attendance from a 5-week pre-pandemic baseline from January 3rd to February 6th, 2020[21].

Google's COVID-19 Open Data repository [22] provides data for daily COVID-19 cases using a consistent set of region keys. Daily values were linked to the 507 cities when city case data was available, matching country-level to cities when city-level data was unavailable. This data was curated by Wahltinez et al. (2020) [23], retrieved directly from the relevant authorities (e.g., departments of health within countries).

Box S4: Air pollution and city mobility changes during COVID-19

Table S1: Relative health risks (and 95% confidence interval) associated with air pollution reductions across continents and phases. Numbers >1 indicate increased health risks.

Region	Early Phase	Mid Phase	Recovery Phase
Mean NO_2 anomaly(ppb) : Estimated Relative Health Risks Due to NO_2 (All-Cause Mortality) (Lower – Upper bound)			
Africa	1.86 : 1.011 (1.007 – 1.015)	0.72 : 1.004 (1.003 – 1.006)	-0.28 : 0.998 (0.999 – 0.998)
Asia	-4.66 : 0.972 (0.981 – 0.963)	-2 : 0.988 (0.992 – 0.984)	-1.58 : 0.991 (0.994 – 0.987)
Europe	-2.81 : 0.983 (0.989 – 0.978)	-3.31 : 0.98 (0.987 – 0.974)	-2.5 : 0.985 (0.99 – 0.98)
North America	-0.48 : 0.997 (0.998 – 0.996)	-1.29 : 0.992 (0.995 – 0.99)	-0.09 : 0.999 (1 – 0.999)
Oceania	-0.22 : 0.999 (0.999 – 0.998)	-3.04 : 0.982 (0.988 – 0.976)	-2.72 : 0.984 (0.989 – 0.978)
South America	-1.23 : 0.993 (0.995 – 0.99)	-2.77 : 0.983 (0.989 – 0.978)	-1.39 : 0.992 (0.994 – 0.989)
Overall	-3.72 : 0.978 (0.985 – 0.97)	-2.15 : 0.987 (0.991 – 0.983)	-1.58 : 0.991 (0.994 – 0.987)
Mean NO_2 anomaly(ppb) : Estimated Relative Health Risks Due to NO_2 (Respiratory Disease) (Lower – Upper bound)			
Africa	1.86 : 1.009 (1.004 – 1.015)	0.72 : 1.004 (1.001 – 1.006)	-0.28 : 0.999 (0.999 – 0.998)
Asia	-4.66 : 0.977 (0.991 – 0.963)	-2 : 0.99 (0.996 – 0.984)	-1.58 : 0.992 (0.997 – 0.987)
Europe	-2.81 : 0.986 (0.994 – 0.978)	-3.31 : 0.983 (0.993 – 0.974)	-2.5 : 0.988 (0.995 – 0.98)
North America	-0.48 : 0.998 (0.999 – 0.996)	-1.29 : 0.994 (0.997 – 0.99)	-0.09 : 1 (1 – 0.999)
Oceania	-0.22 : 0.999 (1 – 0.998)	-3.04 : 0.985 (0.994 – 0.976)	-2.72 : 0.986 (0.995 – 0.978)
South America	-1.23 : 0.994 (0.998 – 0.99)	-2.77 : 0.986 (0.994 – 0.978)	-1.39 : 0.993 (0.997 – 0.989)
Overall	-3.72 : 0.981 (0.993 – 0.97)	-2.15 : 0.989 (0.996 – 0.983)	-1.58 : 0.992 (0.997 – 0.987)
Mean NO_2 anomaly(ppb) : Estimated Relative Health Risks Due to NO_2 (Cardiovascular Disease) (Lower – Upper bound)			
Africa	1.86 : 1.02 (1.013 – 1.03)	0.72 : 1.008 (1.005 – 1.012)	-0.28 : 0.997 (0.998 – 0.996)
Asia	-4.66 : 0.949 (0.967 – 0.925)	-2 : 0.978 (0.986 – 0.968)	-1.58 : 0.983 (0.989 – 0.975)
Europe	-2.81 : 0.969 (0.98 – 0.955)	-3.31 : 0.964 (0.977 – 0.947)	-2.5 : 0.972 (0.982 – 0.96)
North America	-0.48 : 0.995 (0.997 – 0.992)	-1.29 : 0.986 (0.991 – 0.979)	-0.09 : 0.999 (0.999 – 0.999)
Oceania	-0.22 : 0.998 (0.998 – 0.996)	-3.04 : 0.967 (0.979 – 0.951)	-2.72 : 0.97 (0.981 – 0.956)
South America	-1.23 : 0.986 (0.991 – 0.98)	-2.77 : 0.97 (0.981 – 0.956)	-1.39 : 0.985 (0.99 – 0.978)
Overall	-3.72 : 0.959 (0.974 – 0.94)	-2.15 : 0.976 (0.985 – 0.966)	-1.58 : 0.983 (0.989 – 0.975)
Mean $PM_{2.5}$ anomaly($\mu g/m^3$) : Estimated Relative Health Risks Due to $PM_{2.5}$ (All-Cause Mortality) (Lower – Upper bound)			
Africa	-1 : 0.98 (0.986 – 0.974)	-4.1 : 0.917 (0.942 – 0.892)	-4.92 : 0.901 (0.931 – 0.871)
Asia	-13.18 : 0.734 (0.814 – 0.653)	-3.63 : 0.927 (0.949 – 0.905)	-5.99 : 0.879 (0.916 – 0.842)
Europe	-1.49 : 0.97 (0.979 – 0.961)	-1.76 : 0.964 (0.975 – 0.954)	-0.76 : 0.985 (0.989 – 0.98)
North America	-0.61 : 0.988 (0.991 – 0.984)	-0.27 : 0.995 (0.996 – 0.993)	2.47 : 1.05 (1.035 – 1.065)
Oceania	-1.04 : 0.979 (0.985 – 0.973)	-0.93 : 0.981 (0.987 – 0.976)	-2.22 : 0.955 (0.969 – 0.942)
South America	-0.74 : 0.985 (0.99 – 0.981)	-1.73 : 0.965 (0.976 – 0.955)	-0.15 : 0.997 (0.998 – 0.996)
Overall	-9.35 : 0.811 (0.868 – 0.754)	-2.89 : 0.942 (0.959 – 0.924)	-4.04 : 0.918 (0.943 – 0.894)
Mean $PM_{2.5}$ anomaly($\mu g/m^3$) : Estimated Relative Health Risks Due to $PM_{2.5}$ (IHD Mortality) (Lower – Upper bound)			
Africa	-1 : 1 (1 – 1)	-4.1 : 0.999 (1 – 0.998)	-4.92 : 0.999 (1 – 0.998)
Asia	-13.18 : 0.997 (0.999 – 0.995)	-3.63 : 0.999 (1 – 0.999)	-5.99 : 0.999 (0.999 – 0.998)
Europe	-1.49 : 1 (1 – 0.999)	-1.76 : 1 (1 – 0.999)	-0.76 : 1 (1 – 1)
North America	-0.61 : 1 (1 – 1)	-0.27 : 1 (1 – 1)	2.47 : 1.001 (1 – 1.001)
Oceania	-1.04 : 1 (1 – 1)	-0.93 : 1 (1 – 1)	-2.22 : 0.999 (1 – 0.999)
South America	-0.74 : 1 (1 – 1)	-1.73 : 1 (1 – 0.999)	-0.15 : 1 (1 – 1)
Overall	-9.35 : 0.998 (0.999 – 0.996)	-2.89 : 0.999 (1 – 0.999)	-4.04 : 0.999 (1 – 0.998)
Mean $PM_{2.5}$ anomaly($\mu g/m^3$) : Estimated Relative Health Risks Due to $PM_{2.5}$ (Asthma) (Lower – Upper bound)			
Africa	-1 : 0.95 (0.98 – 0.93)	-4.1 : 0.795 (0.918 – 0.713)	-4.92 : 0.754 (0.902 – 0.656)
Asia	-13.18 : 0.341 (0.736 – 0.077)	-3.63 : 0.818 (0.927 – 0.746)	-5.99 : 0.7 (0.88 – 0.581)
Europe	-1.49 : 0.926 (0.97 – 0.896)	-1.76 : 0.912 (0.965 – 0.877)	-0.76 : 0.962 (0.985 – 0.947)
North America	-0.61 : 0.97 (0.988 – 0.957)	-0.27 : 0.986 (0.995 – 0.981)	2.47 : 1.124 (1.049 – 1.173)
Oceania	-1.04 : 0.948 (0.979 – 0.927)	-0.93 : 0.954 (0.981 – 0.935)	-2.22 : 0.889 (0.956 – 0.845)
South America	-0.74 : 0.963 (0.985 – 0.948)	-1.73 : 0.914 (0.965 – 0.879)	-0.15 : 0.992 (0.997 – 0.99)
Overall	-9.35 : 0.532 (0.813 – 0.346)	-2.89 : 0.855 (0.942 – 0.798)	-4.04 : 0.798 (0.919 – 0.717)
Mean $PM_{2.5}$ anomaly($\mu g/m^3$) : Estimated Relative Health Risks Due to $PM_{2.5}$ (IHD Morbidity) (Lower – Upper bound)			
Africa	-1 : 1 (1 – 1)	-4.1 : 0.999 (0.999 – 0.999)	-4.92 : 0.999 (0.999 – 0.998)
Asia	-13.18 : 0.996 (0.997 – 0.996)	-3.63 : 0.999 (0.999 – 0.999)	-5.99 : 0.998 (0.999 – 0.998)
Europe	-1.49 : 1 (1 – 1)	-1.76 : 1 (1 – 0.999)	-0.76 : 1 (1 – 1)
North America	-0.61 : 1 (1 – 1)	-0.27 : 1 (1 – 1)	2.47 : 1.001 (1.001 – 1.001)
Oceania	-1.04 : 1 (1 – 1)	-0.93 : 1 (1 – 1)	-2.22 : 0.999 (1 – 0.999)
South America	-0.74 : 1 (1 – 1)	-1.73 : 1 (1 – 0.999)	-0.15 : 1 (1 – 1)
Overall	-9.35 : 0.997 (0.998 – 0.997)	-2.89 : 0.999 (0.999 – 0.999)	-4.04 : 0.999 (0.999 – 0.999)

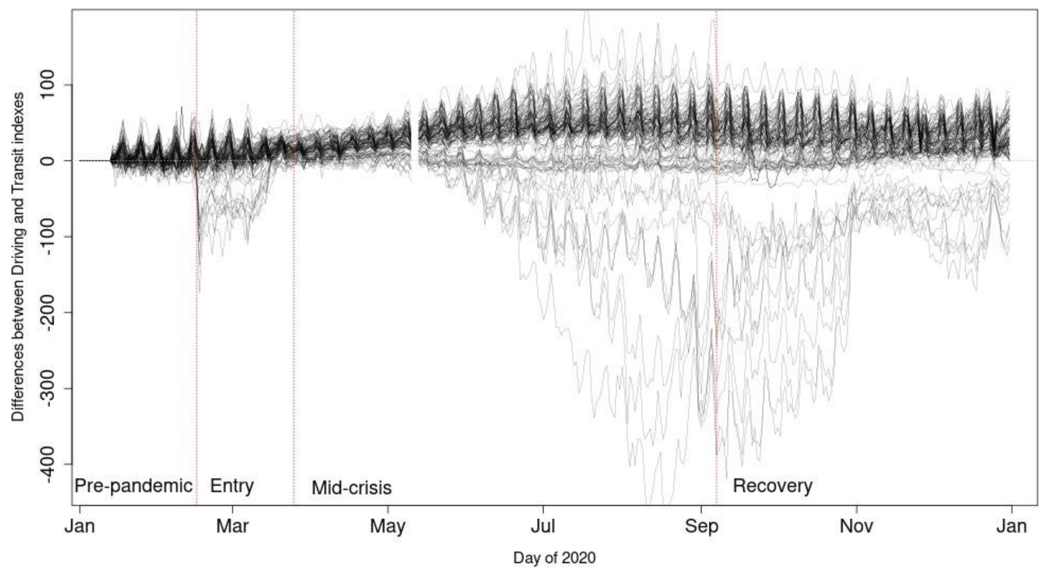

Figure S5: An overview of observed modal shift from public transit to private motor vehicles observed during 2020 for all analysed cities highlighting an increased reliance on private vehicle use over public transit during the course of the COVID-19 pandemic. Values >0 indicate a proportional replacement of public transit trips to private vehicles for individual cities in comparison to pre-pandemic conditions.

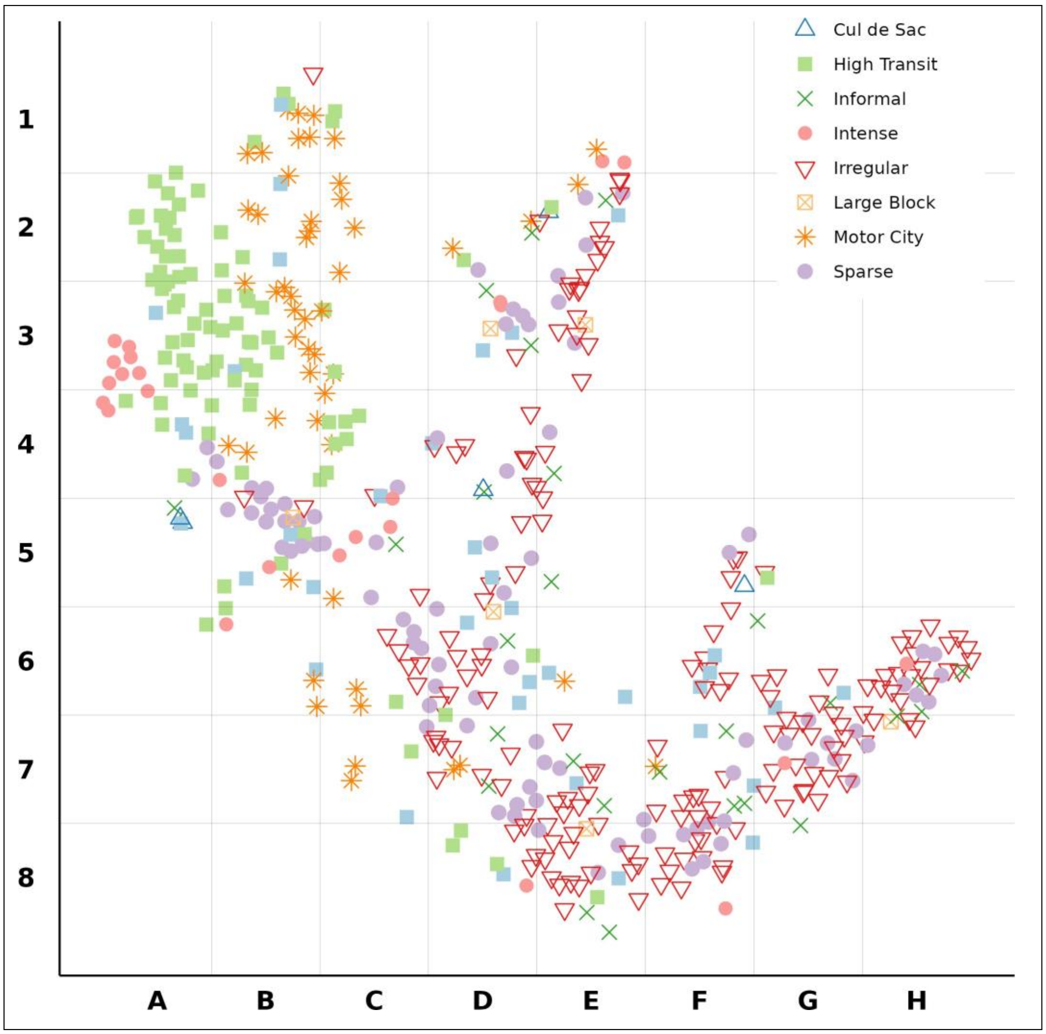

Figure S6: Nine global city design types identified in Thompson et al. (2020)[6] for the 507 cities used in this study. City locations and grid references correspond to those in Figure 1

.

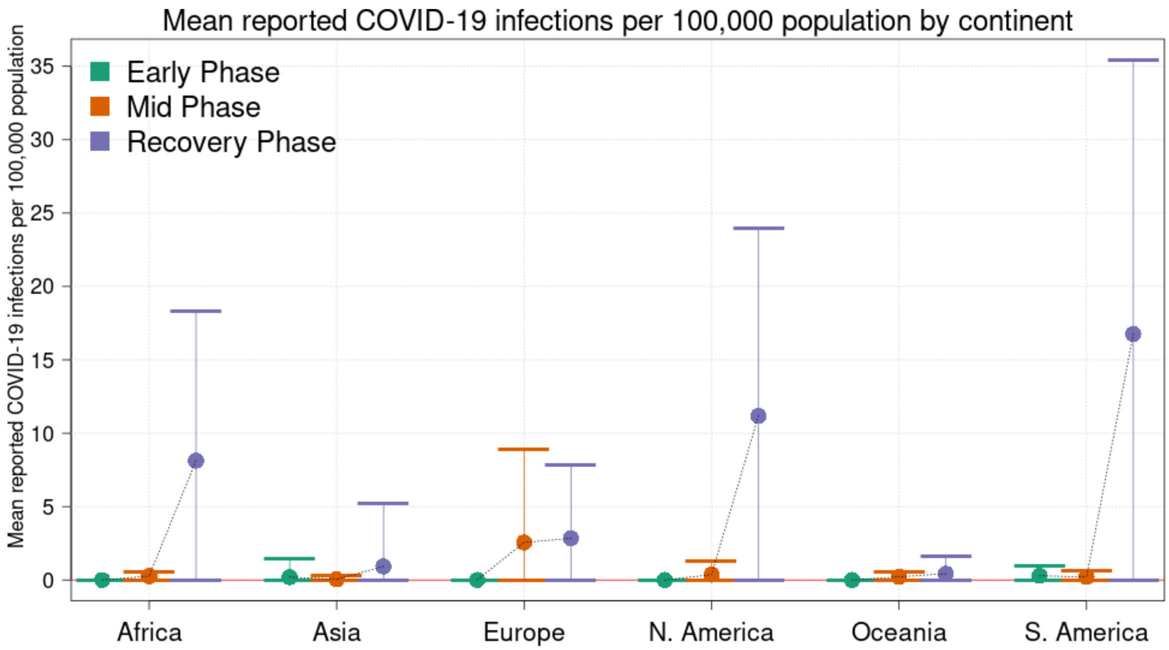

Figure S7: Mean reported COVID-19 cases per 100,000 population across continents in 2020 for the Early, Mid-Crisis, and Recovery pandemic phases with error bars representing standard deviations across countries within regions.

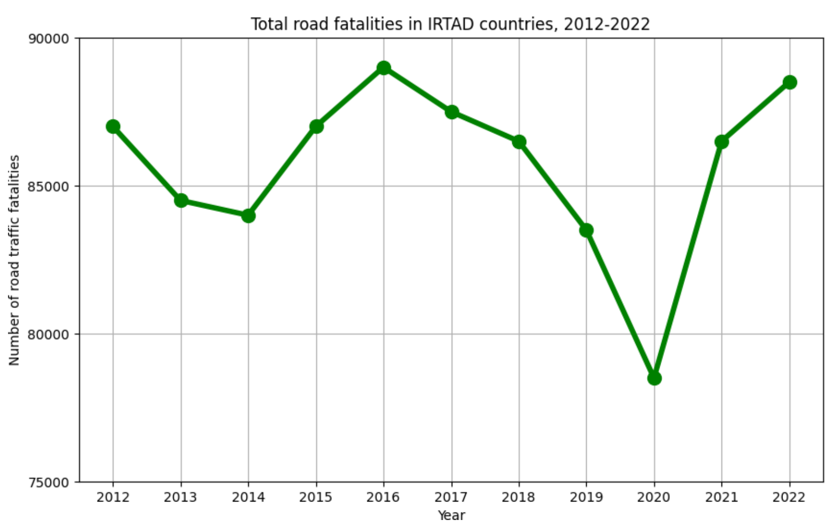

Figure S8: Changes in total road traffic fatalities among the 43 member countries contributing to the International Traffic Safety Data and Analysis Group (IRTAD) showing a post-pandemic (2020-2021) rebound (figure adapted from [24]).

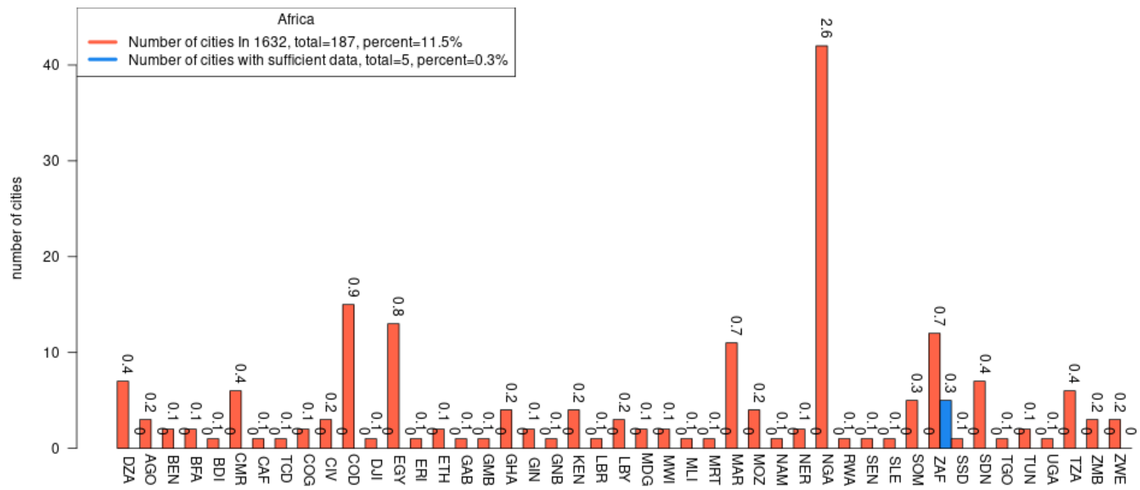

Figure S9: Number of the largest 1632 global cities in countries and the number of cities after excluding cities with insufficient data in Africa. Text annotations show proportions of total (in percents) for each country.

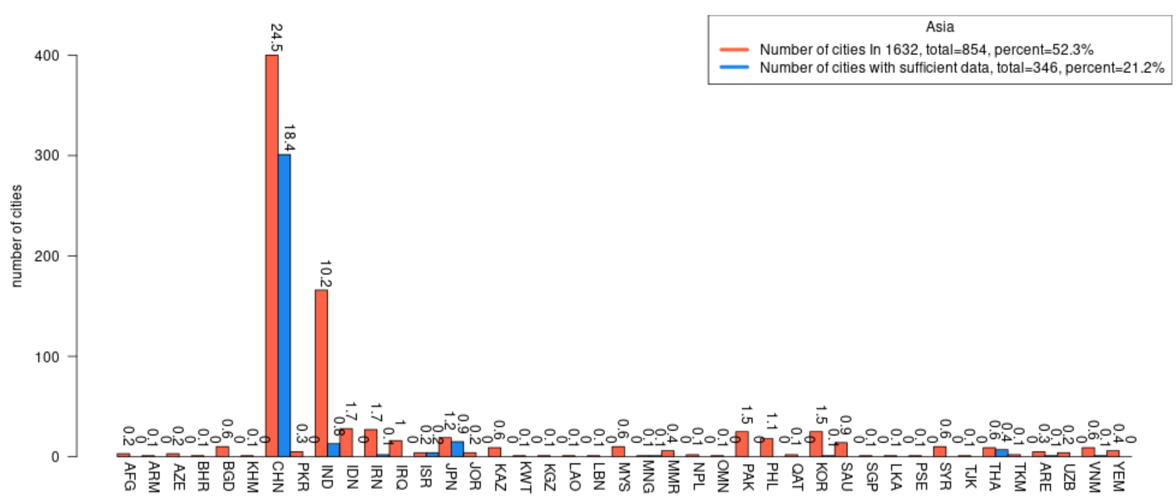

Figure S10: Number of the largest 1632 global cities in countries and the number of cities after excluding cities with insufficient data in Asia. Text annotations show proportions of total (in percents) for each country.

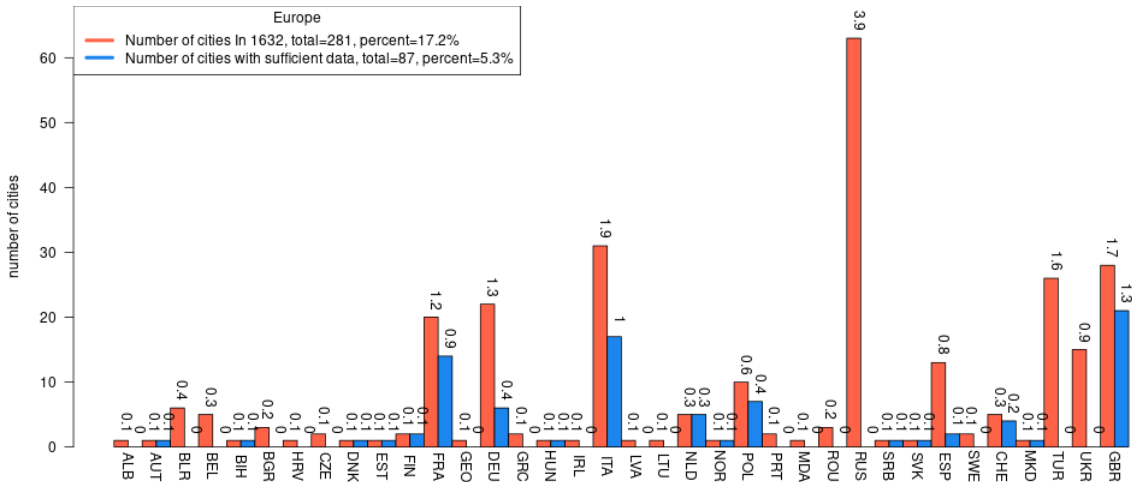

Figure S11: Number of the largest 1632 global cities in countries and the number of cities after excluding cities with insufficient data in Europe. Text annotations show proportions of total (in percents) for each country.

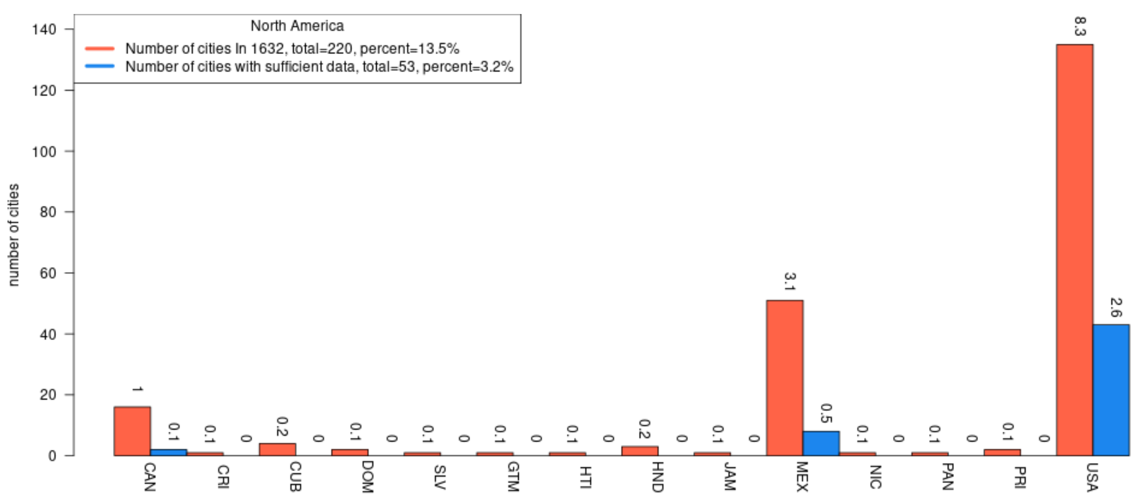

Figure S12: Number of the largest 1632 global cities in countries and the number of cities after excluding cities with insufficient data in North America. Text annotations show proportions of total (in percents) for each country.

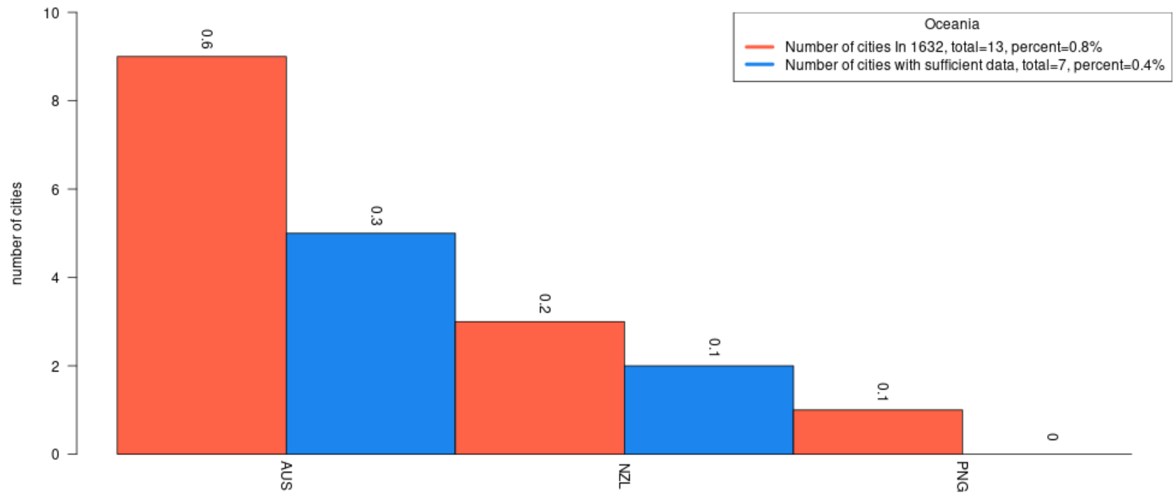

Figure S13: Number of the largest 1632 global cities in countries and the number of cities after excluding cities with insufficient data in Oceania. Text annotations show proportions of total (in percents) for each country.

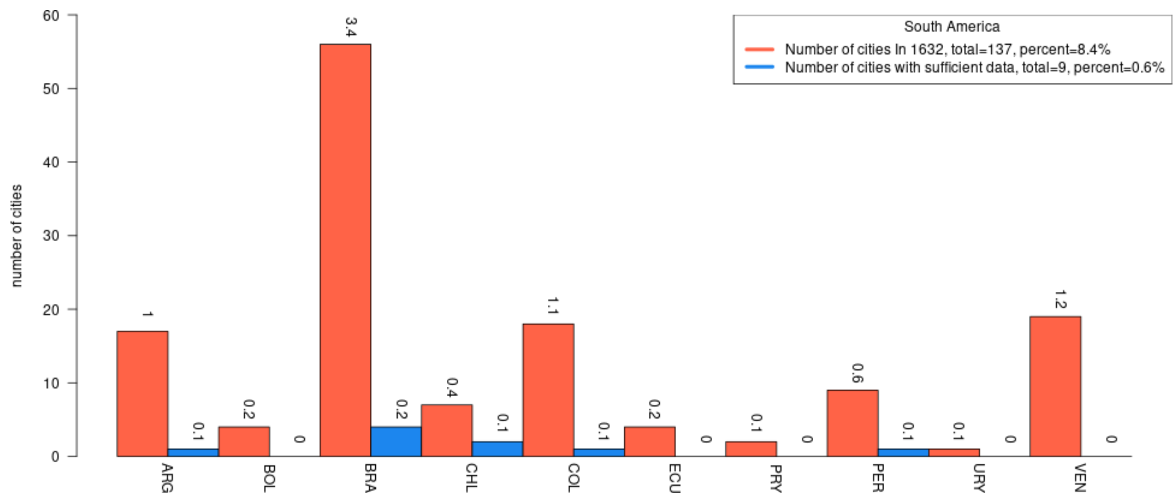

Figure S14: Number of the largest 1632 global cities in countries and the number of cities after excluding cities with insufficient data in South America. Text annotations show proportions of total (in percents) for each country.

References

[1] P. Liu, F. Biljecki, A review of spatially-explicit GeoAI applications in Urban Geography, International Journal of Applied Earth Observation and Geoinformation 112 (2022) 102936. doi:10.1016/j.jag.2022.102936.
URL https://linkinghub.elsevier.com/retrieve/pii/S1569843222001339

[2] S. De Sabbata, Andrea Ballatore, Pengyuan Liu, Nicholas J. Tate, Learning urban form through unsupervised graph-convolutional neural networks, in: The 2nd International Workshop on Geospatial Knowledge Graphs and GeoAI: Methods, Models, and Resources,12th September, 2023, Leeds, UK, 2023. doi:10.17605/OSF.IO/H2AWQ.

[3] J. Xue, N. Jiang, S. Liang, Q. Pang, T. Yabe, S. V. Ukkusuri, J. Ma, Quantifying the spatial homogeneity of urban road networks via graph neural networks, Nature Machine Intelligence 4 (3) (2022) 246–257. doi:10.1038/s42256-022-00462-y.
URL https://www.nature.com/articles/s42256-022-00462-y

[4] Y. Zhang, P. Liu, F. Biljecki, Knowledge and topology: A two layer spatially dependent graph neural networks to identify urban functions with time-series street view image, ISPRS Journal of Photogrammetry and Remote Sensing 198 (2023) 153–168. doi:10.1016/j.isprsjprs.2023.03.008.
URL https://linkinghub.elsevier.com/retrieve/pii/S0924271623000680

[5] T. H. Silva, D. Silver, Using graph neural networks to predict local culture, Environment and Planning B: Urban Analytics and City Science (2024) 23998083241262053doi:10.1177/23998083241262053.
URL https://journals.sagepub.com/doi/10.1177/23998083241262053

[6] J. Thompson, M. Stevenson, J. S. Wijnands, K. A. Nice, G. D. P. A. Aschwanden, J. Silver, M. Nieuwenhuijsen, P. Rayner, R. Schofield, R. Hariharan, C. N. Morrison, A global analysis of urban design types and road transport injury: an image processing study, Lancet Planetary Health 4 (2020) 32–42. doi:10.1016/S2542-5196(19)30263-3.

[7] S. Seneviratne, K. A. Nice, J. S. Wijnands, M. Stevenson, J. Thompson, Self-supervision. remote sensing and abstraction: Representation learning across 3 million locations, in: 2021 Digital Image Computing: Techniques and Applications (DICTA), IEEE, 2021, pp. 01–08.

[8] Q. Zhou, S. Wang, Y. Liu, Exploring the accuracy and completeness patterns of global land-cover/land-use data in OpenStreetMap, Applied Geography 145 (2022) 102742. doi:10.1016/j.apgeog.2022.102742.

[9] Q. Zhou, Y. Zhang, K. Chang, M. A. Brovelli, Assessing OSM building completeness for almost 13,000 cities globally, International Journal of Digital Earth 15 (1) (2022) 2400–2421. doi:10.1080/17538947.2022.2159550.

[10] E. Taillanter, M. Barthelemy, Evolution of road infrastructure in large urban areas, Physical Review E 107 (034304) (2023). doi:10.1103/PhysRevE.107.034304.

[11] Z. Hou, X. Liu, Y. Cen, Y. Dong, H. Yang, C. Wang, J. Tang, Graphmae: Self-supervised masked graph autoencoders, in: Proceedings of the 28th ACM SIGKDD Conference on Knowledge Discovery and Data Mining, 2022, pp. 594–604.

[12] K. He, X. Chen, S. Xie, Y. Li, P. Dolla´r, R. Girshick, Masked autoencoders are scalable vision learners, in: Proceedings of the IEEE/CVF Conference on Computer Vision and Pattern Recognition, 2022, pp. 16000–16009.

[13] S. Seneviratne, R. Shariffdeen, S. Rasnayaka, N. Kasthuriarachchi, Self-supervised vision transformers for malware detection, IEEE Access 10 (2022) 103121–103135.

[14] J. Devlin, M.-W. Chang, K. Lee, K. Toutanova, Bert: Pre-training of deep bidirectional transformers for language understanding, arXiv preprint arXiv:1810.04805 (2018).

[15] F. Pedregosa, G. Varoquaux, A. Gramfort, V. Michel, B. Thirion, O. Grisel, M. Blondel, P. Prettenhofer, R. Weiss, V. Dubourg, J. Vanderplas, A. Passos, D. Cournapeau, M. Brucher, M. Perrot, E. Duchesnay, Scikit-learn: Machine learning in Python, Journal of Machine Learning Research 12 (2011) 2825–2830.

[16] United Nations, Department of Economic and Social Affairs, Population Division, World Urbanization Prospects: The 2014 Revision (2014).
URL https://population.un.org/wup/

[17] J. S. Wijnands, K. A. Nice, S. Seneviratne, J. Thompson, M. Stevenson, The impact of the COVID-19 pandemic on air pollution: A global assessment using machine learning techniques, Atmospheric Pollution Research 13 (6) (2022) 101438. doi:10.1016/j.apr.2022.101438.

[18] H. Hersbach, B. Bell, P. Berrisford, S. Hirahara, A. Hora´nyi, J. Nicolas, C. Peubey, R. Radu, M. Bonavita, D. Dee, R. Dragani, J. Flemming, R. Forbes, A. Geer, R. J. Hogan, H. M. Janiskova´, S. Keeley, P. Laloyaux, P. L. Cristina, J.-n. The´paut, The ERA5 global reanalysis, Quarterly Journal of the Royal Meteorological Society (2020) 1999–2049doi:10.1002/qj.3803.

[19] Apple, Apple Maps Mobility Trends Reports (2020).
URL https://covid19-static.cdn-apple.com/mobility

[20] Google, Google COVID-19 Community Mobility Reports (2020).
URL https://www.google.com/covid19/mobility/

[21] E. Mathieu, H. Ritchie, L. Rode´s-Guirao, C. Appel, C. Giattino, J. Hasell, B. Macdonald, S. Dattani, D. Beltekian, E. Ortiz-Ospina, M. Roser, Coronavirus Pandemic (COVID-19), Our World in Data (2020).
URL https://ourworldindata.org/coronavirus

[22] Google, COVID-19 Open Data. Available at https://github.com/GoogleCloudPlatform/covid-19-open-data (2022).

[23] O. ”Wahltinez, et al.”, ”COVID-19 Open-Data: curating a fine-grained, global-scale data repository for SARS-CoV-2” (2020).
URL https://goo.gle/covid-19-open-data

[24] Road safety annual report 2023, OECD Publishing (2023).